Materials and Design 186 (2020) 108221

Contents lists available at ScienceDirect

Materials and Design

journal homepage: www.elsevier.com/locate/matdes

Nanoparticle additions promote outstanding fracture toughness and fatigue strength in a cast Al–Cu alloy

Chenglin Yang [b,c,1], Qinglong Zhao [a,1], Zhenjun Zhang [b,***], Linlin Li [b,d], Weisi Tian [a], Rui Liu [b], Peng Zhang [b], Yijiang Xu [e], Yanjun Li [e], Zhefeng Zhang [b,c,*], Qichuan Jiang [a,**], Robert O. Ritchie [f]

[a] Key Laboratory of Automobile Materials, Ministry of Education and School of Materials Science and Engineering, Jilin University, No. 5988 Renmin Street, Changchun, 130025, PR China
[b] Materials Fatigue and Fracture Division, Institute of Metal Research, Chinese Academy of Sciences, 72 Wenhua Road, Shenyang, 110016, PR China
[c] University of Chinese Academy of Sciences, 19 Yuquan Road, Beijing, 100049, PR China
[d] Max-Planck-Straße, 1,40237, Düsseldorf, Germany
[e] Department of Materials Science and Engineering, Norwegian University of Science and Technology, Trondheim, N-7491, Norway
[f] Department of Materials Science and Engineering, University of California Berkeley, Berkeley, CA, 94720, USA

HIGHLIGHTS

- A significant porosity reduction is achieved in Al cast alloy through an in-situ nanoparticle master alloy method.
- This method serves to uniformly add nanoparticles into metal melt and improve the bonding between particles and matrix.
- The addition of TiC nanoparticles impedes the formation of porosity and thus improves the mechanical property of Al alloy.
- The fatigue strength, fracture toughness and elongation of the Al alloy are improved to 114 MPa, 55 MPa $m^{1/2}$ and 12%.
- The mechanism of the mechanical property improvement are revealed with the aid of finite element modeling.

GRAPHICAL ABSTRACT

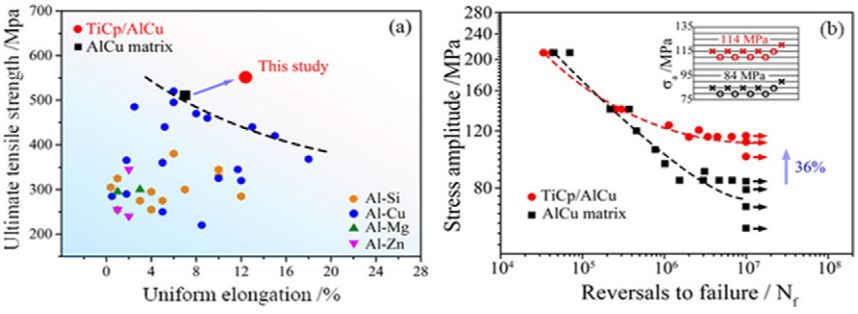

ARTICLE INFO

Article history:
Received 28 July 2019
Received in revised form 4 September 2019
Accepted 17 September 2019
Available online 09 November 2019

Keywords:
Cast Al alloys
Fatigue strength

ABSTRACT

Fatigue resistance and fracture toughness are essential to the reliability of castings during service. Reducing microporosity in cast alloys is a crucial issue for improving their fatigue strength and fracture toughness. Here we report a significant reduction in microporosity of a cast aluminum-copper alloy developed using *in situ* TiC nanoparticle additions coupled with a stir-casting method. The addition of TiC nanoparticles is found to improve the interdendritic feedability of liquid metal and as a result reduces the volume fraction of microporosity by two orders of magnitude compared to a conventionally cast Al–Cu alloy. This method, which is mechanistically associated with a pore-dominated process, acts to significantly improve the fatigue strength, fracture toughness and

* Corresponding author. Materials Fatigue and Fracture Division, Institute of Metal Research, Chinese Academy of Sciences, 72 Wenhua Road, Shenyang, 110016, PR China.
** Corresponding author.
*** Corresponding author.
E-mail addresses: zjzhang@imr.ac.cn (Z. Zhang), zhfzhang@imr.ac.cn (Z. Zhang), jqc@jlu.edu.cn (Q. Jiang).
[1] These authors contributed equally: Chenglin Yang and Qinglong Zhao.

https://doi.org/10.1016/j.matdes.2019.108221

Fracture toughness
Nanoparticles

uniform elongation of the cast Al–Cu alloy to values which, to the best of our knowledge, represent the highest ever achieved for a cast aluminum alloy.

1. Introduction

A persistent quest in the development of lightweight structural materials for the energy-conversion and transportation industries is creating alloys with higher strength and toughness, two properties that are often mutually incompatible. Because of their high strength-to-weight ratio, high on this list are cast aluminum alloys which have many potential applications in the automobile and aerospace industries [1–3]. However, the presence of macro-scale defects (with dimensions above ~10 μm), which form during the casting process, can severely compromise the mechanical properties of these alloys, particularly at higher temperatures [4,5], and as a result cause a marked decrease in the reliability of cast components [6,7]. Accordingly, reducing these macro-scale defects has become a crucial issue for cast aluminum alloys.

Microporosity is one of the major casting defects in these alloys, in that it can significantly reduce ductility and fatigue resistance [8]. This problem can be caused by dendrite growth and solidification shrinkage, usually near the end of the solidification process when limited interdendrtitic liquid flow can no longer compensate for the shrinkage. It is widely accepted that the formation of microporosity is essentially related to the interdendritic feedability (or permeability) and secondary dendrite arm spacing [9,10]. The tortuous interdendritic liquid channels tend to diminish the feedability which serves to escalate the microporosity [10]; conversely, any reduction in the secondary dendrite arm spacing acts to postpone the formation of microporosity [11]. Interestingly, it has been found that the introduction of an inoculant, such as adding Al–Ti–B particles to an 4.5 wt% Cu aluminum alloy, serves to change the dendrite morphology from columnar to equiaxed shape and this changes the pore morphology [12]. Although such particle additions are used to inhibit grain growth during solidification [13,14], their potential use in limiting the degree of microporosity is rarely investigated.

To reveal the effects of adding nanoparticles on the microporosity and mechanical properties of cast Al alloys, an Al–Cu alloy was chosen as the matrix alloy (composition shown in Table 1). TiC particles with a mean diameter of ~97 nm (shown in Fig. 1a) were introduced into the molten alloy through a method of additions of an *in situ* nanoparticle master alloy during stir-casting. The microporosity formation was investigated by *in situ* x-ray radiography with the morphology of the micropores characterized with x-ray tomography (XRT). We found that the presence of the nanoparticles significantly impedes the formation of microporosity and leads to outstanding mechanical properties, compared with those of the currently available cast Al alloys. Admittedly, ceramic particle-reinforced metallic materials (or composites) have been well studied, including their improved mechanical properties [15–17] and particles size effects [18,19]. However, the strengthening mechanisms associated with the addition of TiC nanoparticles in this study lie in a reduction in the microporosity that is quite distinct from the particle reinforcement mechanisms in these early studies.

2. Methods

2.1. Material fabrication

The composition of the Al–Cu matrix alloy used in this study is shown in Table 1. The TiC_p/Al–Cu cast alloy was fabricated by a stir-casting method using an *in situ* nanoparticle master alloy; specifically, nano-sized powders (30–160 nm in diameter) of this TiC_p/Al master alloy were added into the molten Al–Cu matrix alloy during the casting process. The TiC_p/Al master alloy was prepared through combustion synthesis reaction conducted with powders of Al, Ti and carbon nanotubes. The mixed powder was blended by ball milling at a speed of 50 rpm for 48 h and was then cold pressed into cylindrical preforms (28 mm in diameter and 40 mm in height) with a ~65% theoretical density. The combustion synthesis reaction of the preforms was conducted in a vacuum heat-treatment furnace at 1173 K to produce the TiC_p/Al master alloy. The TiC_p/Al master alloy was added into the molten Al–Cu alloy at 1173 K, followed by mechanical stirring for 2 min to distribute the titanium carbide particulate evenly in the matrix. The final fraction of the nano-sized TiC_p was 0.3% by weight. After the molten alloy was cooled down to 1073 K, it was cast into a preheated steel mold ($400 \times 200 \times 50$ mm^3) to form an ingot. The casting process for the matrix Al–Cu alloy was the same as that used for the TiC_p/Al–Cu alloy, as described above. The as-cast grain structures of the matrix Al–Cu and TiC_p/Al–Cu alloys are shown in Fig. 1b and c, respectively.

The ingots were subjected to a T6 heat treatment, *i.e.*, a solution treatment at 811 ± 1 K for 12 h and aging at 438 K for 10 h. Round-bar shaped tensile and fatigue specimens were machined with a gauge diameter and length of respectively 5 mm and 15 mm. Compact-tension C(T) samples were used for the fracture toughness measurements with the dimensions shown in Supplementary Fig. 1. To create a smooth, nominally stress-free surface, the tensile and fatigue specimens were mechanically polished and then the fatigue specimens experienced electro-polishing in a mixed solution of 30 vol% HNO_3 and 70 vol% CH_3OH.

2.2. Microstructure characterization

The surfaces of the electrolytic-polished matrix Al–Cu and TiC_p/Al–Cu alloy samples were observed by a ZEISS Supra 35 scanning electron microscopy (SEM). The internal defects of the two materials were directly characterized with three-dimensional x-ray tomography (3D-XRT) using an Xradia Versa XRM-500 instrument with a resolution of ~1 μm per pixel. The samples for XRT had a 1 mm^2 section with a length of 2 mm. The microstructure of the two materials was investigated using an FEI Tecnai F20 transmission electron microscope operating at 200 kV. Atom probe tomography (APT) specimens were prepared using FEI Helios Plasma focused ion beam, with Xe source to avoid easy Ga implantation [20], using an *in situ* lift-out method [21]. APT measurements were performed on LEAP3000X HR by Cameca in voltage-pulsed mode at 50 K, with a pulse fraction of 15%, a pulse rate of 200 kHz, and a target detection rate of 0.4% (4 detection events per 1000 pulses in average). The reconstruction of 3D atom maps, visualization and all data analysis were performed using the IVAS® software from Imago Scientific Instruments.

Samples examined by x-ray radiography were Al-18 wt%Cu with and without 0.1 wt% of TiC; the *in situ* x-ray radiography facility used for this work is described elsewhere [22,23]. The Cu concentration was increased to 18 wt% to improve the x-ray absorption contrast. Large grains are preferred due to the limited spatial resolution of x-ray radiography (~1.5 μm/pixel), so a minor addition of TiC (0.1 wt%) was selected to demonstrate the effect of TiC on solidification. The casting procedure was the same as that for the TiC_p/Al–Cu alloy. The size of x-ray radiography samples was $50 \times 5 \times 0.18$ mm, as cut from the ingot. The thin foil samples were positioned horizontally on a holder to avoid melt convection. After heating the sample to melt, the furnace was operated in a near-isothermal mode with a cooling rate of 0.1 K/s, and the images were recorded at a frame rate of 1 Hz.

2.3. Mechanical property testing

Room-temperature tensile tests were carried out at a strain rate of 10^{-3} s^{-1} with an Instron 5982 testing machine with the strains measured using an extensometer. High-

Table 1
The nominal composition and micro-hardness of the Al–Cu matrix and TiC_p/Al–Cu alloys.

	TiC	Cu	Mn	Ti	Cd	V	Zr	B	Micro hardness
Matrix	None	5.00%	0.45%	0.30%	0.20%	0.20%	0.15%	0.04%	144 ± 3 Hv
TiC/AlCu	0.30%	5.00%	0.45%	0.30%	0.20%	0.20%	0.15%	0.04%	159 ± 4 Hv

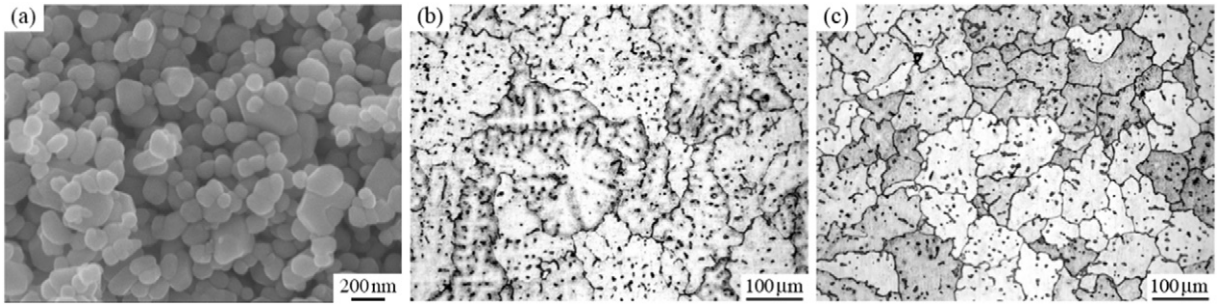

Fig. 1. (**a**) SEM image of TiC nanoparticles extracted from the TiC_p/Al master alloy. Optical metallography of the (**b**) as-cast matrix Al–Cu alloy and (**c**) TiC_p/Al–Cu alloy.

temperature tensile properties were evaluated at four elevated temperatures, namely, 100°, 140°, 180° and 220 °C, using a heating rate and hold time of 20 °C/min and 20 min, respectively. For each condition, three samples were tested to ensure the repeatability and credibility of the results.

Stress-controlled axial pull-push fatigue tests were performed with a stress ratio (ratio of minimum to maximum stress) of $R = -1$ on an Instron 8871 testing machine at a frequency of 40 Hz with a sinusoidal waveform. The fatigue limit (σ_{-1}) was determined for lifetimes exceeding 10^7 cycles using tension-compression testing. Fracture toughness tests were conducted on an Instron 8871 testing machine with three C(T) specimens for each condition. The C(T) specimens were pre-cracked by fatigue and were finally loaded to fracture at a displacement rate of 1 mm/min. The detailed method for computing K_{Ic} values are presented in our previous study [24]. Vickers hardness tests were conducted with an Everone MH-5L hardness tester at 1000 N for 20 s and 10 indentations were made on each specimen.

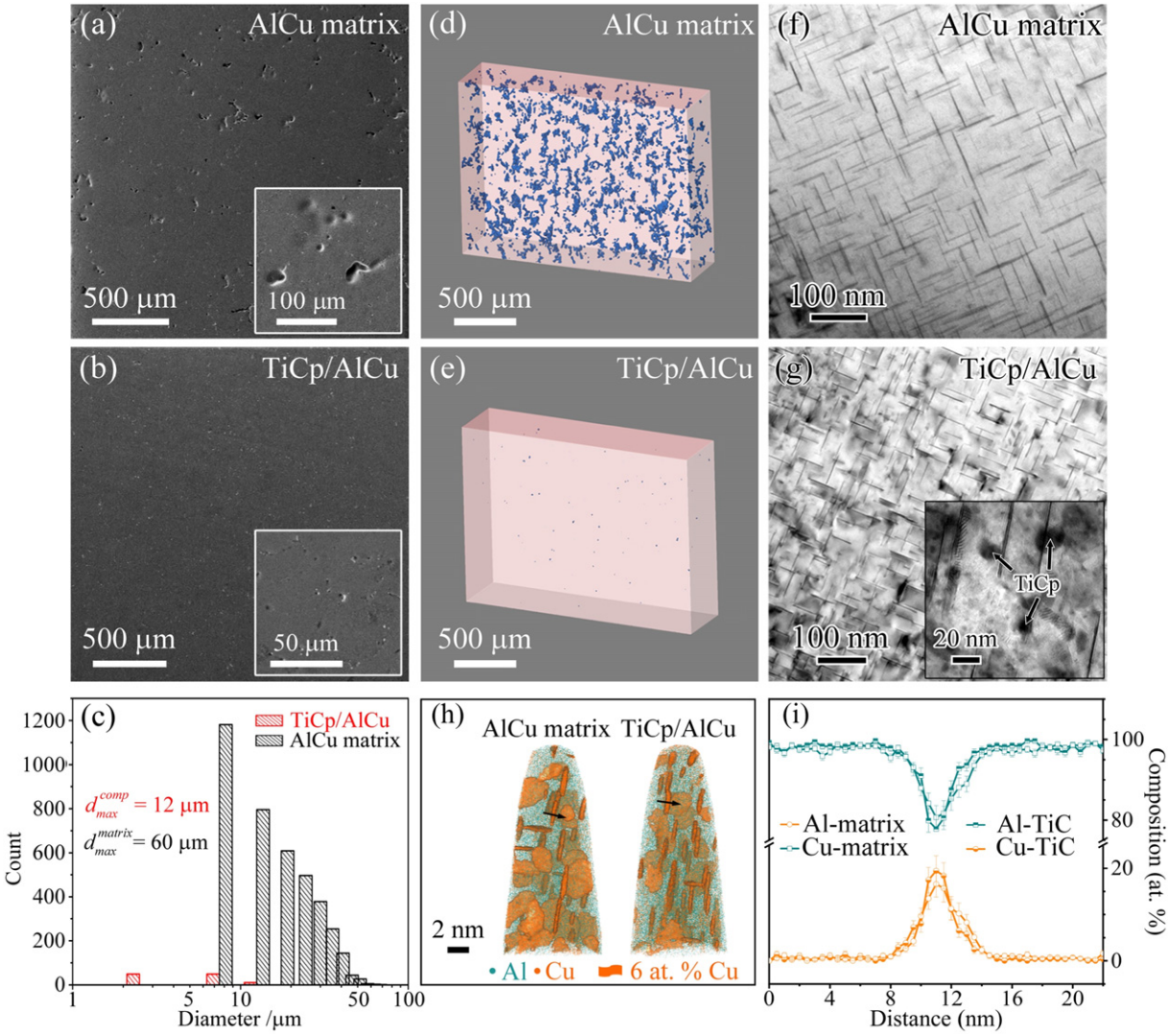

Fig. 2. Microstructures of the Al–Cu matrix and the TiC_p/Al–Cu alloys prior to deformation. The matrix alloy contains significantly more micropores than the TiC_p/Al–Cu alloy, as verified by (**a, b**) SEM sample surface and (**d, e**) bulk XRT observations. (**c**) Quantitative measurements from XRT of the number and size of the voids in the Al–Cu matrix and TiC_p/Al–Cu alloys. (**f, g**) TEM and (**h, i**) Atom Probe tomography (APT) imaging show the size and spacing of the θ' (Al_2Cu) precipitates to be larger in the Al–Cu matrix alloy than in the TiC_p/Al–Cu alloy.

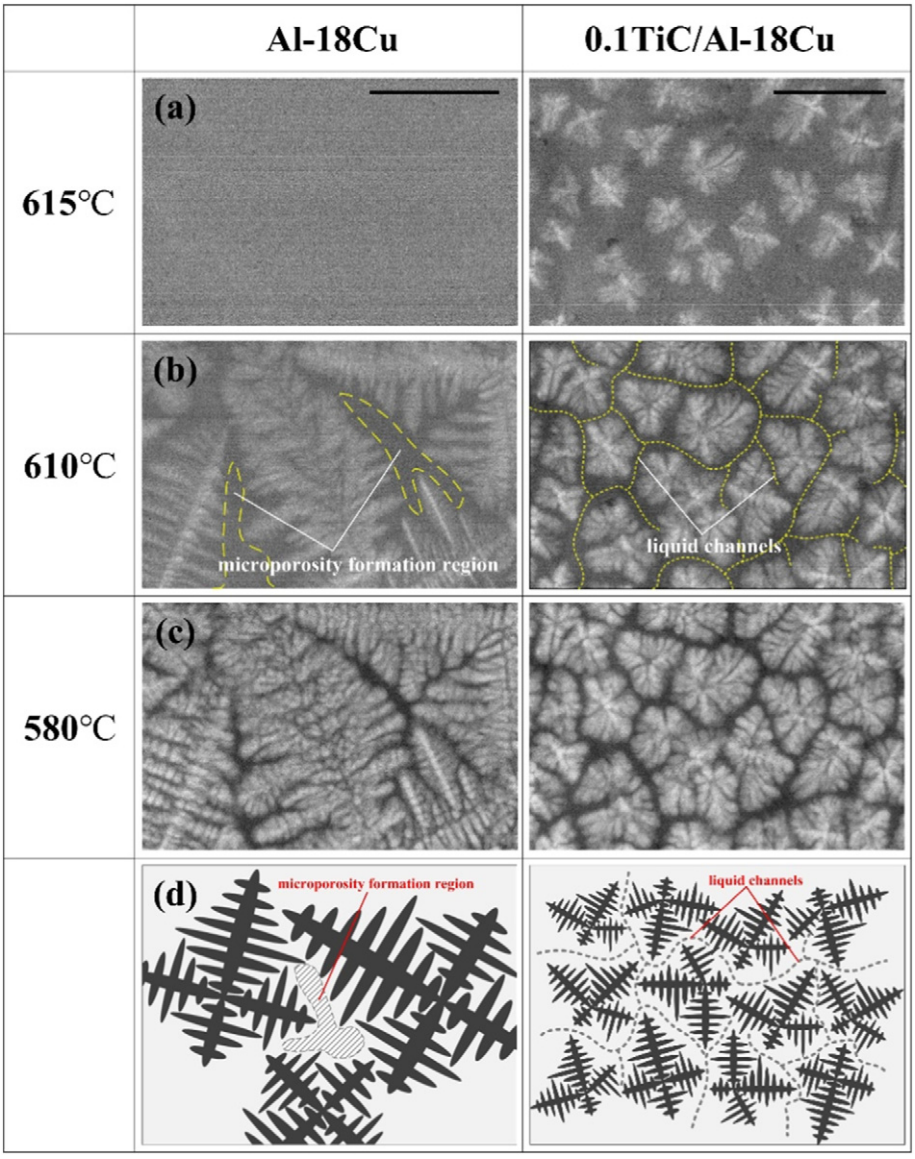

Fig. 3. ***In situ*** **x-ray radiography of the solidification of the model Al–Cu binary alloy and TiC_p/Al–Cu alloy**. Image of the state of solidification at (**a**) 615 °C, (**b**) 610 °C, (**c**) 580 °C (cooling rate 0.1 K/s; scale bar: 1 mm). The isolated liquid region in the Al–Cu binary alloy is indicated by the dashed lines. The liquid channels in the TiC_p/Al–Cu alloy are indicated by the dotted lines. (**d**) Schematics of the microporosity formation in the isolated liquid regions between dendrite arms near the end of solidification, showing the formation of micropores in the Al–Cu alloy and in the residual liquid channels in the TiC_p/Al–Cu alloy.

3. Experimental results

3.1. Microstructure before deformation

Microstructure characterization was performed to verify the reduced size and fraction of micropores caused by the addition of the nano-sized TiC particles. Fig. 2a and b shows scanning electron microscopy (SEM) images of the electro-polished sample surfaces of the matrix Al–Cu alloy and the alloy with TiC nanoparticle additions (TiC_p/Al–Cu), respectively. It is clear that the surface of the matrix alloy is covered with ~50-μm diameter micropores, whereas the corresponding surface of the TiC_p/Al–Cu alloy is characterized by much smoother voids smaller than ~10 μm. The difference in the distribution and size of the micropores in the two materials can be directly verified using XRT. Fig. 2d and e shows the XRT images of the internal defects in the matrix Al–Cu alloy and in the TiC_p/Al–Cu alloy, respectively, with the blue regions indicating the casting defects. Consistent with the SEM observations, there are clearly fewer and smaller micropores in the Al–Cu alloy with TiC particle additions, as shown quantitatively by the count data in Fig. 2c derived from the XRT images. Specifically, the volume fraction of voids in the TiC_p/Al–Cu alloy matrix is less than 0.01%, *i.e.*, over 100 times smaller than in the Al–Cu matrix alloy where it is ~1%. Aside from the marked reduction in macro-scale defects, the microstructure of the alloy is also changed after nano-sized TiC particle additions. Fig. 2f and g shows transmission electron microscopy (TEM) images of the two materials. Precipitates can be observed in both alloys, which have been identified as the θ′ (Al_2Cu) phase in a previous study [25]. Such θ′ precipitates in the Al–Cu matrix alloy were ~100 nm in length with a mean spacing of ~50 nm, whereas those in the TiC_p/Al–Cu alloy were finer and more closely spaced with an average size and spacing of ~50 nm and ~10 nm, respectively. Note that the TiC particles themselves can be as small as ~10 nm (inserted image in Fig. 2g). From reconstructed 3-D atom maps of needle-shaped specimens in Fig. 2h, examined using atom probe tomography, the plate-shape θ′ precipitates can be seen to be highlighted in terms of 6 at.% Cu iso-composition surfaces. There are minor differences in the compositions of the two materials, as displayed by the 1-D concentration profiles along the arrows across a θ′ precipitate in Fig. 2h; these profiles are plotted in Fig. 2i.

The micropores are formed in the liquid region which is constrained by adjacent dendrite arms due to solidification contraction, which for the Al–Cu matrix is ~7% by volume (Supplementary Fig. 2). The TiC particles are intended to act as heterogeneous nucleation sites during the solidification of the Al–Cu because of their good wettability and the small lattice misfit (6.9%) between TiC and Al [26].

The specific effects of TiC nanoparticles on the nucleation and growth of our model Al–Cu binary alloy were investigated using *in situ* x-ray radiography, as shown in Fig. 3a–c. When the Al–Cu liquid is cooled to 615 °C, no α-Al grains were observed to form, in contrast to the many fine equiaxed α-Al grains that had already formed in the TiC_p/Al–Cu alloy (Fig. 3a), which strongly suggests that TiC nanoparticles indeed act to promote heterogeneous nucleation of the α-aluminum. At lower temperatures (610 °C), large α-Al dendrites were observed to grow in the field of view of the Al–Cu binary alloy with some tips of the arms of the α-Al dendrites reaching the adjacent dendrite arms. Here, a large fraction of the liquid was clearly constrained in the interdendritic or intergranular regions, as indicated in Fig. 3b. In contrast, α-Al dendrite arms in the TiC_p/Al–Cu alloy grew

slowly with intergranular liquid channels remaining interconnected; this is also shown in Fig. 3b. As the temperature was further reduced to 580 °C, the solidification process reached completion with the eutectic Al_2Cu phases forming within interdentritic regions and at grain boundaries.

To give an indication of the difference in size, the field of view for our x-ray radiography (2.9 × 1.9 mm) was insufficient to view a complete grain in the Al–Cu matrix alloy, whereas more than twenty equiaxed α-Al grains appeared in the field of view of the TiC_p/Al–Cu alloy (Fig. 3c). Moreover, the size and spacing of the dendrite arms in the TiC_p/Al–Cu alloy were significantly refined compared to the Al–Cu alloy. The formation of micropores in the interdendritic or intergranular regions are illustrated in Fig. 3d. As the dendrite arms in the Al–Cu alloy touch adjacent dendrite arms, the residual liquid flow is constrained by the solid phase network; once the interdendritic or intergranular liquid channels become so enclosed, the liquid flow can no longer compensate for the contraction due to solidification. The result is that micropores then form in the isolated residual liquid left in the interdendritic or intergranular regions. In the Al–Cu matrix alloy, the primary and secondary dendrite arms double in size and cause a higher fraction of liquid to be enclosed in these interdendritic or intergranular regions with the result that the shrinkage micropores that form are also large and concentrated in these regions (Fig. 2d). In contrast, the liquid channels in the TiC_p/Al–Cu alloy are more interconnected and less tortuous due to the suppressed dendrite arm growth and refined grain size. Consequently, the fraction of enclosed liquid in the interdendritic or intergranular regions was much lower than that in the matrix alloy: at 610 °C, the fraction of enclosed liquid region in the matrix and TiC_p/Al–Cu alloy are about 10% and 2%, respectively. X-ray radiography at 600 °C indicated that 58% of the liquid phase was enclosed in the interdendritic regions in the Al–18Cu reference alloy, whereas only 20% was enclosed in TiC_p/Al–18Cu alloy. Here, the interdendritic or intergranular flow is expected to compensate for the shrinkage, thereby inhibiting micropore formation, which in turn result in micropores in the TiC_p/Al–Cu alloy that are fewer in number and smaller in size than those in the matrix alloy.

3.2. Mechanical property testing results

The addition of the TiC particulate to the Al–Cu alloy, which results in markedly different microstructures, correspondingly leads to the differences in the mechanical properties (Figs. 4 and 5). A comparison of the ultimate tensile strength (UTS) and uniform elongation (UE) of the current Al–Cu matrix and TiC_p/Al–Cu alloys with the corresponding properties of several cast Al alloys, including four stir-cast alloys [27], is shown in Fig. 4a. Although cast Al alloys invariably exhibit a trade-off between strength and elongation – higher strength generally results in lower uniform elongation – both Al–Cu alloys examined in this study displayed the best combination of strength and ductility compared to all the conventionally fabricated Al alloys. The TiC_p/Al–Cu alloy, however, exhibits a UTS and uniform elongation of, respectively, ~550 MPa and ~12%, both representing improvements compared to the matrix alloy. The superior mechanical properties generated by the addition of nano-size TiC particles can also be seen in the uniaxial tensile true stress-strain curves shown in Fig. 4b. Although the improvement in yield strength is not significant, the fracture strength increases roughly 100 MPa and the uniform elongation by a factor of two. Furthermore, the TiC_p/Al–Cu alloy also shows superior high-temperature tensile performance compared to the Al–Cu alloy (Fig. 4c), consistent with previous studies [25,26]. The ratio between the strength of the Al–Cu and TiC_p/Al–Cu alloy increases with increasing temperature, that is, the addition of TiC particles has a more apparent effect at high temperature.

Fig. 5 shows the results of the fatigue tests and fracture toughness tests conducted on the matrix Al–Cu and TiC_p/Al–Cu alloys. Stress *vs.* cycles to failure (*S*–*N*) fatigue curves and the measured 10^7-cycle fatigue limits are shown in Fig. 5a where it is apparent that, although the fatigue lives are similar for the two materials at relatively high stress amplitudes, the TiC_p/Al–Cu displays a progressively superior fatigue resistance at decreasing stress amplitudes. In terms of fatigue limits, the addition of the nano-particulate TiC raises the fatigue limit by some 36% from a value of 84 MPa in the matrix alloy to 114 MPa in the TiC_p/Al–Cu alloy.

For comparison, the fatigue strength and UTS of several cast Al alloys, including Al–Si–Mg, Al–Si–Cu and Al–Cu–Mn alloys [27,28] and the two current Al–Cu alloys, are summarized in Fig. 5b. Whereas the fatigue properties of the Al–Cu matrix alloy are similar to those of the other conventionally fabricated alloys, the TiC_p/Al–Cu alloy is distinctly superior. Moreover, with respect to the compendium of fracture toughness and yield strength plotted in Fig. 5c for cast Al alloys, including Al–Zn–Mg, Al–Cu–Mg, Al–Cu–Li, Al-Li-Cu and Al–Si–Mg [29–33], the fracture toughness of the matrix Al–Cu alloy, at 45 MPa·$m^{½}$, is among the highest for conventionally-cast Al alloys, yet the toughness of the TiC_p/Al–Cu alloy is even higher at 55 MPa·$m^{½}$.

4. Discussions

4.1. Improvement in tensile strength and fracture toughness

Based on these results, it is evident that the TiC_p/Al–Cu alloy displays a combination of outstanding tensile and fatigue strength, as well as excellent fracture toughness, without loss in ductility. Although the nano-particulate additions serve to alter the composition and microstructure, such as the change in the θ′ precipitate size, we believe that the major reason for the improvement can be attributed to the reduction in the volume fraction of casting defects and their size. The following sections

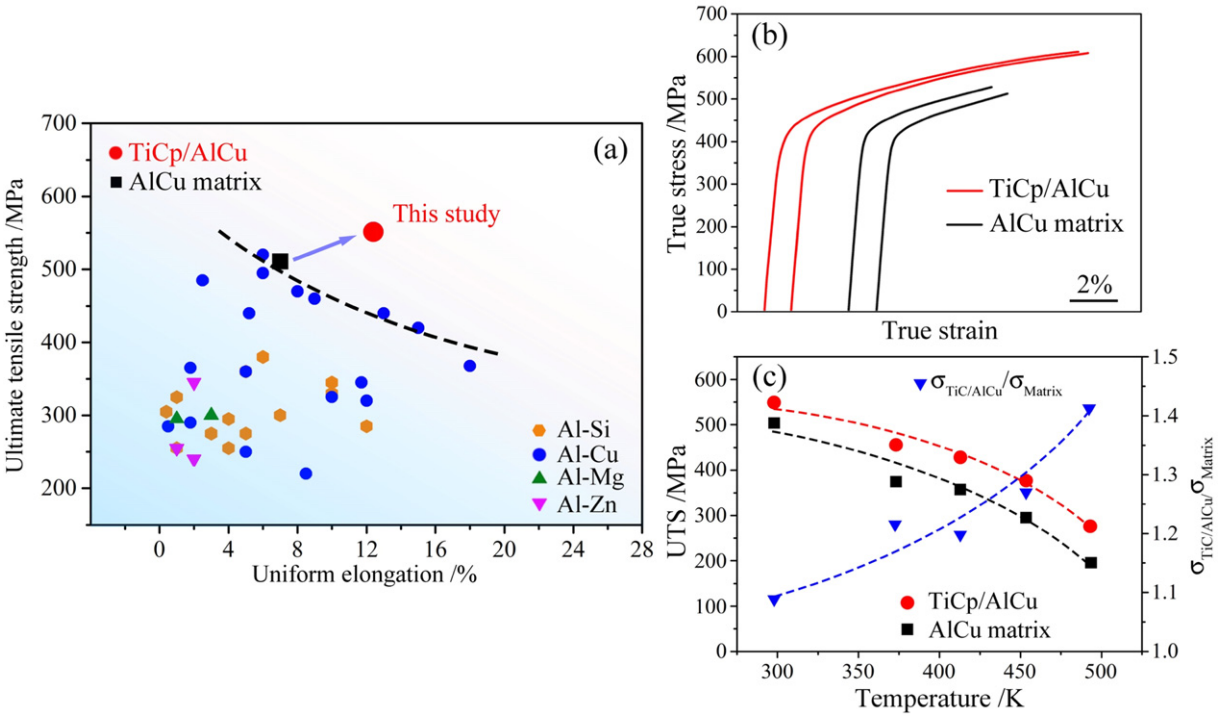

Fig. 4. Uniaxial tensile properties of the Al–Cu matrix and TiC_p/Al–Cu alloys. (**a**) Uniform elongation *vs.* ultimate tensile strength for the current Al–Cu and TiC_p/Al–Cu alloys compared with the corresponding properties of several conventional cast Al alloys[27]; the TiC_p/Al–Cu alloy can be seen to display the best combination of properties. (**b**) Room-temperature tensile stress-strain curves for the Al–Cu matrix and TiC_p/Al–Cu alloys. (**c**) The ultimate tensile strength of the Al–Cu matrix alloy and TiC_p/Al–Cu alloy at different temperatures; the improvement in strength through TiC particle additions can be seen to be more apparent at high temperatures.

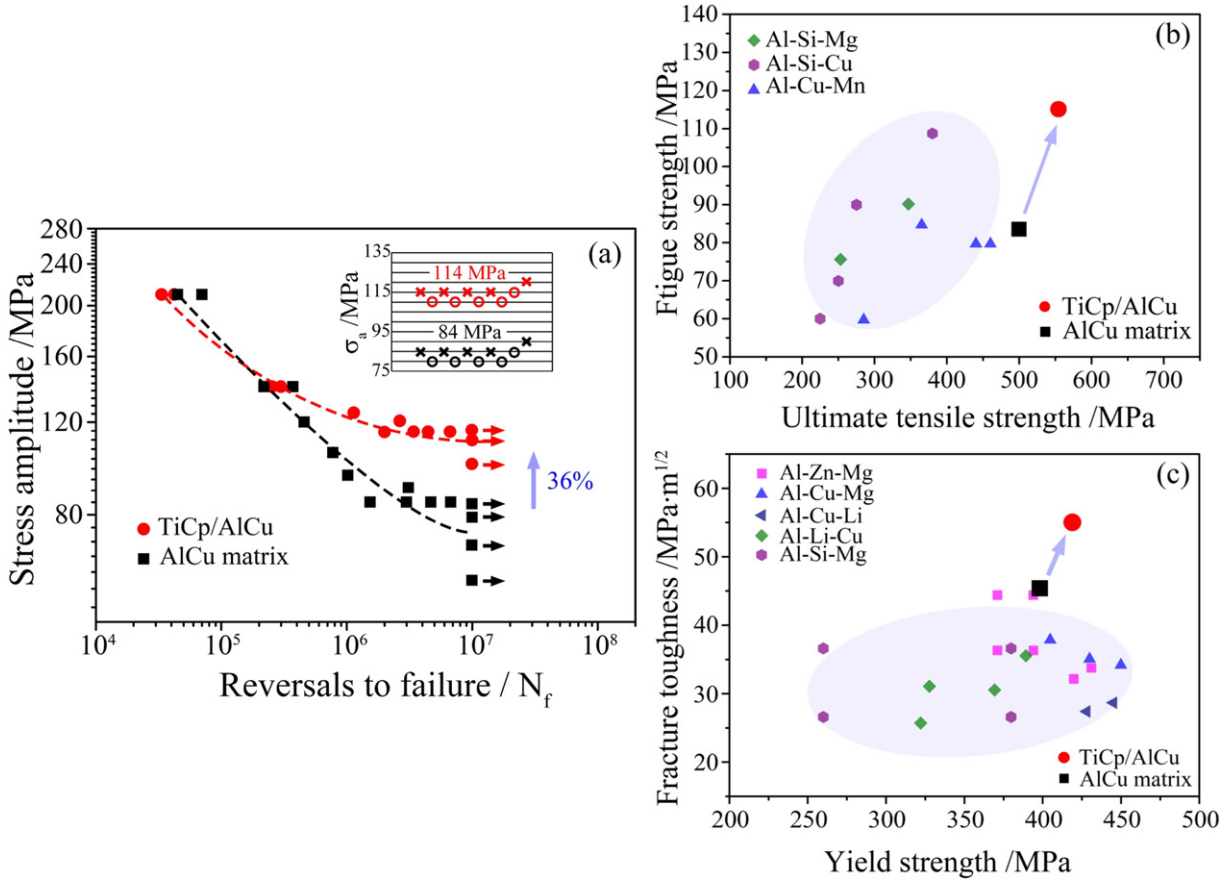

Fig. 5. Fatigue strength and fracture toughness of the Al–Cu matrix and TiC_p/Al–Cu alloys. (**a**) *S–N* fatigue curves and plots of (**b**) ultimate tensile strength *vs.* fatigue strength and (**c**) yield strength *vs.* fracture toughness for the Al–Cu and TiC_p/Al–Cu alloys, compared corresponding data for with conventionally-cast Al alloys[29–33].

now focus on the mechanisms underlying these improved mechanical properties.

Firstly, the improvement in the tensile strength and fracture toughness from TiC nanoparticle additions can be directly attributed to the reduction in the amount and size of the micropores. Although both the matrix alloy and the TiC_p/Al–Cu alloy fail by a nominally flat fracture, *i.e.*, with fracture angles of nearly 90° to the tensile axis, shown in Supplementary Fig. 3, the reduction in the load-bearing area caused by larger porosity cannot explain the difference in tensile strength between the Al–Cu matrix and TiC_p/Al–Cu alloys: the real normal stress inside the specimens can be calculated as

$$s = \frac{\sigma A}{A - A_v}, \tag{1}$$

where σ is the true stress obtained through tensile tests, A is the cross-section area of the entire specimen and A_v is the total cross section area of the micropores. At fracture, the A_v of the matrix Al–Cu alloy and the TiC_p/Al–Cu alloy are estimated to be 0.046*A* and 0.002*A*, respectively, according to the XRT data, with the fracture strengths measured as 525 MPa and 610 MPa, respectively, from the results of the tensile tests. Substituting the values of A_v and fracture strength into Eq. (1), one can obtain the true normal stress of the two materials, *i.e.*, 550 MPa and 611 MPa. Clearly, even after subtracting the area represented by the microporosity, which naturally cannot carry load, the normal stress to cause fracture of the matrix Al–Cu alloy is still lower than that of the TiC_p/Al–Cu alloy. Thus, the maximum normal stress is not the dominate mechanism of the final tensile fracture.

As cast Al alloys usually fail by void coalescence [34], the larger size and amount of the micropores in the Al–Cu matrix alloy would promote earlier fracture and result in a larger gap between the true stress-strain and the strain-hardening rate curves (as shown in Fig. 6). Therefore, observations that the TiC_p/Al–Cu alloy exhibits a higher tensile strength and ductility is consistent with its fewer and smaller micropores. Such a reduction in the size and distribution of micropores induced by the TiC nanoparticulate additions is also consistent with the improved fracture toughness of this cast alloy. Specifically, the larger and more numerous pre-existing micropores in the matrix Al–Cu alloy would serve to exacerbate the process of microvoid coalescence and thereby accelerate cracking, resulting in a reduced stress required for final fracture and a lower fracture toughness.

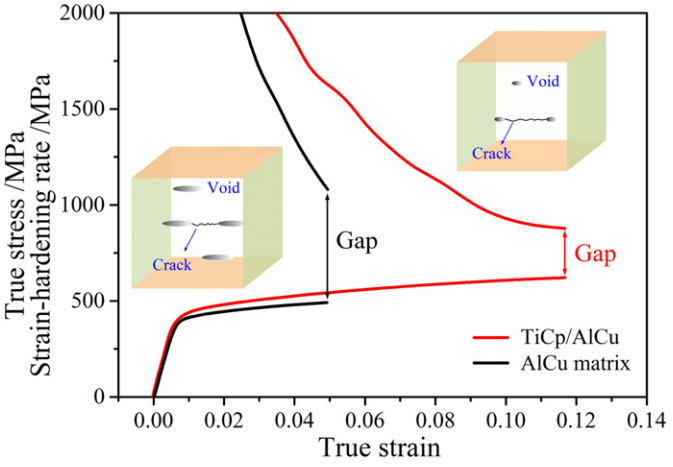

Fig. 6. Tensile fracture of the Al–Cu matrix and TiC_p/Al–Cu alloys. For both alloys, the strain-hardening rate and true stress-strain curves do not intersect, which indicates a fracture dominated by voids coalescence.

4.2. Improvement in fatigue strength

The improvement in fatigue resistance of the cast Al–Cu alloy can also be attributed to the reduction of the microporosity due to TiC particulate additions. From the *S–N* (Wöhler) curves shown in Fig. 5a, improvement in the fatigue lifetimes (at a given stress amplitude) for the TiC_p/Al–Cu alloy, compared to the matrix Al–Cu alloys, only occurs at longer lives, primarily exceeding ~5×10^{-5} cycles. In this longer life regime, fatigue lifetimes are invariably dominated by crack initiation, as opposed to crack growth [35,36], again consistent with the diminished role of micropores in the TiC_p/Al–Cu alloy in promoting the formation of incipient fatigue cracks. Evidence that indeed fatigue cracks do initiate from the micropores in both the Al–Cu matrix and TiC_p/Al–Cu alloys can be seen in Fig. 7. The addition of TiC particles effectively reduces the size and amount of the micropores, which serves as the initiation point of fatigue crack. Thus, with less and small pores, the TiC_p/Al–Cu alloy is more resistant to fatigue crack initiation, which leads to a longer fatigue life. In contrast, the matrix Al–Cu alloy with more and larger pores is more vulnerable to fatigue crack initiation and thus present a shorter fatigue life. An approximate relationship between the micropore defects and the resulting fatigue limit can be deduced using the empirical approach of Murakami and Endo [37], *viz.*:

$$\sigma_w = \frac{\alpha(Hv + 120)}{\left(\sqrt{Area}\right)^{1/6}}. \tag{2}$$

The average Vickers hardness *Hv* of the matrix Al–Cu alloy and the TiC_p/Al–Cu alloy was 144 Hv and 159 Hv, respectively, based on 10 indentations. The *Area* for the matrix Al–Cu alloy and the TiC_p/Al–Cu alloy was 2826 μm^2 and 113 μm^2, respectively, calculated through $Area = \pi\,(d/2)^2$ where *d* is the size of the largest micropore listed in Fig. 1c. As for the factor α, it can be considered as a constant, because the fatigue cracks of the two materials initiate at the same sites, *i.e.*, from the micropores on the sample surface. Substituting the above parameters into Eq. (1), one obtains the ratio of the fatigue limits of the two alloys to be ~0.71. This estimation is consistent with the experimentally measured ratio 0.73 (84 MPa/114 MPa, as shown in Fig. 4a). The bottom line here is that the improvement in the fatigue strength can be related to the addition of nano-sized TiC particles which acts to suppress the generation and growth of micropores; this in turn reduces the potency of fatigue crack initiation sites in the cast Al–Cu alloy, thereby elevating the longer life fatigue strength of the TiC_p/Al–Cu alloy compared to that of the Al–Cu matrix alloy.

5. Conclusions

To summarize, the cast Al–Cu alloy processed using *in situ* TiC nanoparticle additions coupled with a stir-casting method display a combination of outstanding mechanical properties in comparison with to the cast aluminum alloys currently available: the ultimate tensile strength and uniform elongation reach 550 MPa and 12%, the fatigue strength increases by 36% (from 84 MPa to 114 MPa) relative to the matrix alloy without TiC nanoparticle additions and the fracture toughness is similarly increased to K_{Ic} ~ 55 MPa·m^{½}. Such excellent strength, ductility, fatigue and toughness properties of the TiC_p/Al–Cu alloy are attributed to a marked reduction in the size and extent of casting microporosity, which serves to aid the tensile alloy's strength, but more importantly to provide a lesser contribution to microvoid coalescence thereby enhancing the ductility and toughness; furthermore, the smaller and less numerous micropores diminish the opportunity

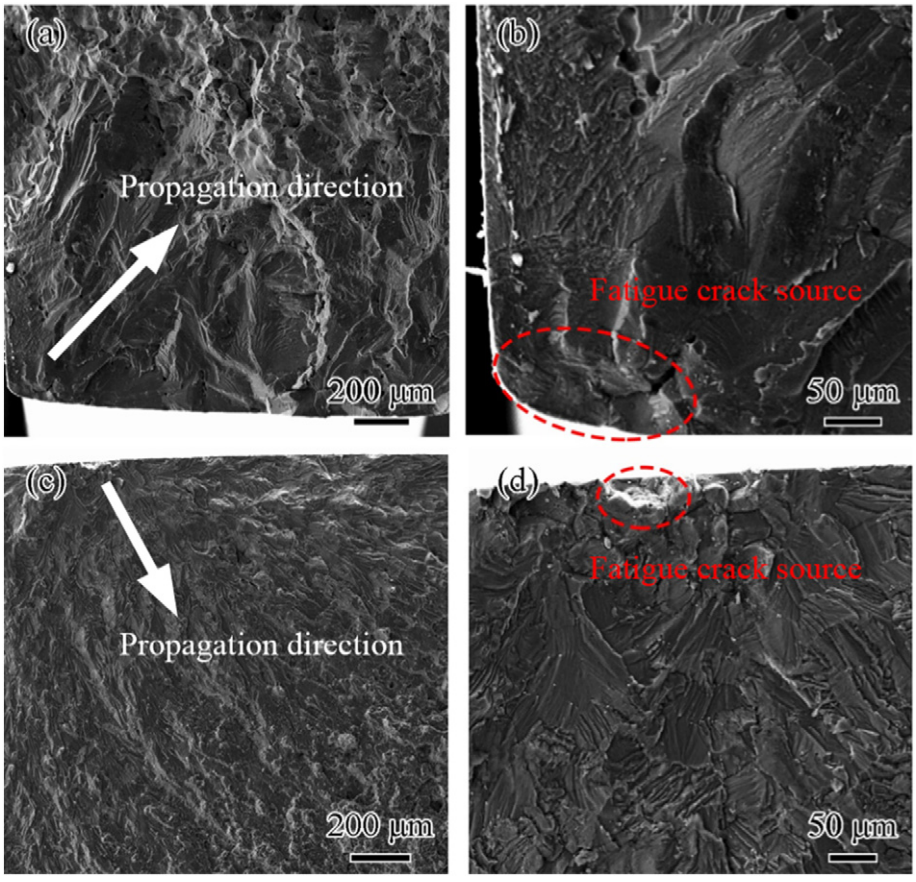

Fig. 7. SEM images of the fatigue fracture surfaces of (**a**), (**b**) the matrix Al–Cu, and (**c**), (**d**) the TiC_p/Al–Cu alloys after ~10^6 cycles under 92 MPa and 124 MPa, respectively. For both materials, the fatigue cracks initiate from micropores on the sample surface, as shown by the dashed-line circles.

for the premature initiation of fatigue cracks, leading to a significant improvement in high-cycle fatigue resistance.

CRediT authorship contribution statement

Chenglin Yang: Data curation, Formal analysis, and Writing original draft.**Qinglong Zhao:** Data curation and Formal analysis.**Zhenjun Zhang:** Supervision.**Linlin Li:** Methodology.**Weisi Tian:** Methodology. **Rui Liu:** Data curation and Formal analysis.**Peng Zhang:** Data curation and Formal analysis.**Yijiang Xu:** Methodology.**Yanjun Li:** Methodology.**Zhefeng Zhang:** Conceptualization, Funding acuisition, Writing - original draft, and Supervision. **Qichuan Jiang:** Conceptualization, Funding acuisition, Writing - original draft. **Robert O. Ritchie:** Writing - original draft and Writing - review & editing.

Acknowledgements

This work was supported by the sponsor-id="https://doi.org/10.13039/501100001809">National Natural Science Foundation of China (NSFC) under grant nos. 51790483, 51790482 and 51871223, 51330007. The authors would like to thank Drs. Dierk Raabe and Baptiste Gault for their sound suggestions and inspiring discussion.

Appendix A. Supplementary data

Supplementary data to this article can be found online at https://doi.org/10.1016/j.matdes.2019.108221.

Competing financial interests

The authors declare no competing financial interests.

References

[1] E. Salahi, A. Rajabi, Fabrication and characterisation of copper-alumina nanocomposites prepared by high-energy fast milling, Mater. Sci. Technol. 32 (2016) 1212–1217.
[2] Z. Wang, C. Li, H. Wang, X. Zhu, M. Wu, J. Li, Q. Jiang, Aging behavior of nano-SiC/2014Al composite fabricated by powder metallurgy and hot extrusion techniques, J. Mater. Sci. Technol. 32 (2016) 1008–1012.
[3] M. Li, H. Wang, Z. Wei, Z. Zhu, The effect of Y on the hot-tearing resistance of Al–5wt.% Cu based alloy, Mater. Des. 31 (2010) 2483–2487.
[4] C.H. Caceres, B.I. Selling, Casting defects and the tensile properties of an Al-Si-Mg alloy, Mater. Sci. Eng. A 220 (1996) 109–116.
[5] J.A. Francis, G.M.D. Cantin, The role of defects in the fracture of an Al-Si-Mg cast alloy, Mater. Sci. Eng. A 407 (2005) 322–329.
[6] C. Booth-Morrison, D.N. Seidman, D.C. Dunand, Effect of Er additions on ambient and high-temperature strength of precipitation-strengthened Al-Zr-Sc-Si alloys, Acta Mater. 60 (2012) 3643–3654.
[7] M. Zamani, S. Seifeddine, A.E.W. Jarfors, High temperature tensile deformation behavior and failure mechanisms of an Al-Si-Cu-Mg cast alloy - the microstructural scale effect, Mater. Des. 86 (2015) 361–370.
[8] J.M. Boileau, J.E. Allison, The effect of solidification time and heat treatment on the fatigue properties of a cast 319 aluminum alloy, Metall. Mater. Trans. A 34 (2003) 1807–1820.
[9] R.G. Santos, M.L.N.M. Melo, Permeability of interdendritic channels, Mater. Sci. Eng. A 391 (2005) 151–158.
[10] E. Khajeh, D.M. Maijer, Physical and numerical characterization of the near-eutectic permeability of aluminum–copper alloys, Acta Mater. 58 (2010) 6334–6344.
[11] Y. Liu, W. Jie, Z. Gao, Y. Zheng, Investigation on the formation of microporosity in aluminum alloys, J. Alloy. Comp. 629 (2015) 221–229.
[12] M. Felberbaum, M. Rappaz, Curvature of micropores in Al–Cu alloys: an X-ray tomography study, Acta Mater. 59 (2011) 6849–6860.
[13] K. Wang, H.Y. Jiang, Y.W. Jia, H. Zhou, Q.D. Wang, B. Ye, W.J. Ding, Nanoparticle-inhibited growth of primary aluminum in Al–10Si alloys, Acta Mater. 103 (2016) 252–263.
[14] A.L. Greer, Overview: application of heterogeneous nucleation in grain-refining of metals, J. Chem. Phys. 145 (2016) 211704.
[15] D. Zhou, F. Qiu, Q. Jiang, The nano-sized TiC particle reinforced Al–Cu matrix composite with superior tensile ductility, Mater. Sci. Eng. A 622 (2015) 189–193.
[16] W.S. Tian, D.S. Zhou, F. Qiu, Q.C. Jiang, Superior tensile properties of in situ nano-sized TiCp/Al-Cu composites fabricated by reaction in melt method, Mater. Sci. Eng. A 658 (2016) 409–414.
[17] D.S. Zhou, J. Tang, F. Qiu, J.G. Wang, Q.C. Jiang, Effects of nano-TiCp on the microstructures and tensile properties of TiCp/Al–Cu composites, Mater. Char. 94 (2014) 80–85.
[18] L. Zhang, F. Qiu, J. Wang, Q. Jiang, High strength and good ductility at elevated temperature of nano-SiCp/Al2014 composites fabricated by semi-solid stir casting combined with hot extrusion, Mater. Sci. Eng. A 626 (2015) 338–341.
[19] M. Bahrami, K. Dehghani, M.K.B. Givi, A novel approach to develop aluminum matrix nano-composite employing friction stir welding technique, Mater. Des. 53 (2014) 217–225.
[20] Y. Xiao, J. Wehrs, H. Ma, T. Al-Samman, S. Korte-Kerzel, M. Göken, J. Michler, R. Spolenak, J.M. Wheeler, Investigation of the deformation behavior of aluminum micropillars produced by focused ion beam machining using Ga and Xe ions, Scr. Mater. 127 (2017) 191–194.
[21] G.B. Thompson, M.K. Miller, H.L. Fraser, Some aspects of atom probe specimen preparation and analysis of thin film materials, Ultramicroscopy 100 (2004) 25–34.
[22] H. Nguyen-Thi, G. Reinhart, G.S.A. Jaoude, R. Mathiesen, G. Zimmermann, Y. Houltz, D. Voss, A. Verga, D. Browne, A.G. Murphy, XRMON-GF: a novel facility for solidification of metallic alloys with in situ and time-resolved X-ray radiographic characterization in microgravity conditions, J. Cryst. Growth 374 (2013) 23–30.
[23] Y. Xu, D. Casari, Q. Du, R.H. Mathiesen, L. Arnberg, Y.J.A.M. Li, Heterogeneous nucleation and grain growth of inoculated aluminium alloys: an integrated study by in-situ X-radiography and numerical modelling, Acta Mater. 140 (2017) 224–239.
[24] H.F. Li, Q.Q. Duan, P. Zhang, R.T. Qu, Z.F. Zhang, A new method to estimate the plane strain fracture toughness of materials, Fatigue Fract. Eng. Mater. Struct. 42 (2019) 415–424.
[25] W. Tian, Q. Zhao, Q. Zhang, F. Qiu, Q. Jiang, Superior creep resistance of 0.3 wt% nano-sized TiCp/Al-Cu composite, Mater. Sci. Eng. A 700 (2017) 42–48.
[26] W. Tian, Q. Zhao, Q. Zhang, F. Qiu, Q. Jiang, Simultaneously increasing the high-temperature tensile strength and ductility of nano-sized TiCp reinforced Al-Cu matrix composites, Mater. Sci. Eng. A 717 (2018) 105–112.
[27] F.S. Pan, D.F. Zhang, Aluminum Alloy and its Applications, Chemical Industry Press, Beijing, 2006.
[28] S.H. Kim, K.-S. Kim, K.S. Cho, K.J. Euh, Y.M. Rhyim, K.-A. Lee, Effect of heat treatment on the tensile and high-cycle fatigue properties of A356 casting alloy, Korean J. Metal. Mater. 53 (2015) 96–103.
[29] C. Qin, G.Q. Gou, X.L. Che, H. Chen, J. Chen, P. Li, W. Gao, Effect of composition on tensile properties and fracture toughness of Al–Zn–Mg alloy (A7N01S-T5) used in high speed trains, Mater. Des. 91 (2016) 278–285.
[30] Q. Zhao, Z. Liu, T. Huang, P. Xia, F. Li, Enhanced fracture toughness in an annealed Al-Cu-Mg alloy by increasing Goss/Brass texture ratio, Mater. Char. 119 (2016) 47–54.
[31] E.D. Sweet, C.G. Bennett, I. Musulin, S.P. Lynch, R.B. Nethercott, Effects of alkali-metal impurities on fracture toughness of 2090 Al-Li-Cu extrusions, Metall. Mater. Trans. A 27 (1996) 3530–3541.
[32] C.J. Gilbert, R.O. Ritchie, W.L. Johnson, Fracture toughness and fatigue-crack propagation in a Zr-Ti-Ni-Cu-Be bulk metallic glass, Appl. Phys. Lett. 71 (1997) 476–478.
[33] V. Kumar, I.V. Singh, B.K. Mishra, R. Jayaganthan, Improved fracture toughness of cryorolled and room temperature rolled 6082 Al alloys, Acta Metall. Sin. Engl. Lett. 27 (2014) 359–367.
[34] R.O. Ritchie, A.W. Thompson, On macroscopic and microscopic analyses for crack initiation and crack growth toughness in ductile alloys, Metall. Trans. A 16 (1985) 233–248.
[35] W. Li, T. Sakai, M. Wakita, S. Mimura, Influence of microstructure and surface defect on very high cycle fatigue properties of clean spring steel, Int. J. Fatigue 60 (2014) 48–56.
[36] D. Spriestersbach, A. Brodyanski, J. Loesch, M. Kopnarski, E. Kerscher, Very high cycle fatigue of bearing steels with artificial defects in vacuum, Mater. Sci. Technol. 32 (2016) 1111–1118.
[37] Y. Murakami, M. Endo, Effects of defects, inclusions and inhomogeneities on fatigue-strength, Int. J. Fatigue 16 (1994) 163–182.